



1 **Heterogeneous photochemistry of imidazole-2-**
2 **carboxaldehyde: HO₂ radical formation and aerosol growth**
3 **Laura González Palacios^{1,2}, Pablo Corral Arroyo^{3,4}, Kifle Z. Aregahegn^{5,6} Sarah S.**
4 **Steimer^{3,4,7}, Thorsten Bartels-Rausch³, Barbara Nozière⁵ Markus Ammann^{3,4},**
5 **Christian George⁵ and Rainer Volkamer^{1,2}**

6 [1]{University of Colorado, Department of Chemistry and Biochemistry, 215 UCB, Boulder,
7 CO, 80309, USA }

8 [2]{University of Colorado, Cooperative Institute for Research in Environmental Sciences
9 (CIRES), 216 UCB, Boulder, CO, 80309, USA }

10 [3]{Paul Scherrer Institute, Laboratory of Radio- and Environmental Chemistry, 5232 Villigen
11 PSI, Switzerland }

12 [4]{Swiss Federal Institute of Technology Zurich, Institute for Atmospheric and Climate
13 Science, 8092 Zürich, Switzerland }

14 [5]{Université Lyon 1; Centre National de la Recherche Scientifique (CNRS), UMR5256,
15 IRCELYON, Institut de recherches sur la catalyse et l'environnement de Lyon, F-69626
16 Villeurbanne, France }

17 [6]{now at: Chemistry Department, University of California, Irvine, California, 92697-202 }

18 [7]{now at: University of Cambridge, Department of chemistry, Cambridge CB2 1EW, UK }

19 Correspondence to: R. Volkamer (rainer.volkamer@colorado.edu).

20

21 **Abstract**

22 The multiphase chemistry of glyoxal is a source of secondary organic aerosol (SOA), including its
23 light-absorbing product imidazole-2-carboxaldehyde (IC). IC is a photosensitizer that can
24 contribute to additional aerosol ageing and growth when its excited triplet state oxidizes
25 hydrocarbons (reactive uptake) via H-transfer chemistry. We have conducted a series of
26 photochemical coated-wall flow tube (CWFT) experiments using films of IC and citric acid (CA),
27 an organic proxy and H-donor in the condensed-phase. The formation rate of gas-phase HO₂



28 radicals (P_{HO_2}) was measured indirectly by converting gas-phase NO into NO_2 . We report on
29 experiments that relied on measurements of NO_2 formation, NO loss; and HONO formation. P_{HO_2}
30 was found to be a linear function of (1) the $[IC] \times [CA]$ concentration product, and (2) the photon
31 actinic flux. Additionally, (3) a more complex function of relative humidity ($25\% < RH < 63\%$),
32 and of (4) the O_2/N_2 ratio ($15\% < O_2/N_2 < 56\%$) was observed, most likely indicating competing
33 effects of dilution, HO_2 mobility and losses in the film. The maximum P_{HO_2} was observed at 25-
34 55% RH and at ambient O_2/N_2 . The HO_2 radicals form in the condensed-phase when excited IC
35 triplet states are reduced by H-transfer from a donor, CA in our system, and subsequently react
36 with O_2 to re-generate IC, leading to a catalytic cycle. OH does not appear to be formed as a
37 primary product but is produced from the reaction of NO with HO_2 in the gas phase. Further, seed
38 aerosols containing IC and ammonium sulfate were exposed to gas-phase limonene and NO_x in
39 aerosol flow tube experiments, confirming significant P_{HO_2} from aerosol surfaces. Atmospheric
40 implications consist in a potentially relevant contribution of triplet state photochemistry for gas-
41 phase HO_2 production, aerosol growth and ageing.

42

43 1. Introduction

44 The sources and sinks of radicals play an important role in the oxidative capacity of the
45 atmosphere. Radicals and other oxidants initiate the chemical degradation of various trace gases,
46 which is key in the troposphere (Jacob, 1999). The hydroxyl (OH) and peroxy (HO_2) radicals
47 belong to the HO_x chemical family and are primarily generated by ultraviolet radiation
48 photochemical reactions (Calvert and Pitts, 1966), like the reaction of $O(^1D)$ (from O_3) with H_2O ,
49 or photolysis of HONO, HCHO, H_2O_2 , or acetone. Some secondary gas-phase sources are the
50 ozonolysis of alkenes or $O(^1D) + CH_4$ (Monks, 2005). The oxidation of VOCs by OH and other
51 oxidants in the presence of NO leads to perturbations in the HO_x , NO_x , and RO_x radical cycles that
52 affect O_3 and aerosol formation (Monks, 2005; Sheehy et al., 2010). The kinetics and
53 photochemical parameters of these reactions are relatively well-known in the gas-phase (Atkinson
54 et al., 2004; Sander et al., 2011). However, this does not apply to the sources and sinks for HO_x
55 in atmospheric droplets and on aerosol surfaces (Ervens et al., 2011). Uptake of OH from the gas-
56 phase, and H_2O_2 photolysis in the condensed phase are the primary known sources for HO_x in the
57 condensed-phase. HO_2 is highly soluble and the concentrations of OH, the most effective oxidant



58 in the condensed phase, depend on HO₂. Another source of HO_x radicals is from the chemical
59 reactions of reduced metal ions and H₂O₂, known as Fenton reactions (Fenton, 1894; Deguillaume
60 et al., 2005). Direct photolysis of H₂O₂, nitrite, nitrate (Zellner et al., 1990), hydroperoxides (Zhao
61 et al., 2013), and light absorbing secondary organic aerosol (SOA) (Badali et al., 2015) are also
62 sources of HO_x in the condensed-phase. Other studies have shown that the photochemistry of iron
63 (III) oxalate and carboxylate complexes, present in aqueous environments (e.g. wastewater,
64 clouds, fogs, particles), can initiate a radical chain reaction serving as an aqueous source of HO₂
65 and Fe²⁺. Fe²⁺ can then regenerate OH starting a new cycle of Fenton reactions (Weller et al.,
66 2013a, 2013b). The temperature dependent rate constants of OH in the aqueous phase have been
67 studied for a limited subset of organics (Ervens et al., 2003). However, there is still a wide gap
68 with respect to understanding the sources, sinks, kinetics and photochemical reaction pathways of
69 HO_x radicals in the condensed phase (George et al., 2015).

70 Our study investigates photosensitizers as an additional HO_x source that may be relevant to further
71 modify RO_x and NO_x reaction cycles in both the condensed- and gas-phases. It is motivated by
72 the formation of superoxide in terrestrial aqueous photochemistry (Draper and Crosby, 1983;
73 Faust, 1999; Schwarzenbach et al., 2002), by more recent observations that irradiated surfaces
74 containing titanium dioxide generate HO_x radicals in the gas-phase (Yi et al., 2012) and by the
75 generation of OH from metal oxides acting as photocatalysts in mineral dust (Dupart et al., 2012).
76 Past studies have demonstrated the reactivity of glyoxal towards ammonium ions and amines as a
77 source for light-absorbing brown carbon (Nozière et al., 2009; Galloway et al., 2009; Shapiro et
78 al., 2009; Kampf et al., 2012). One of these products is imidazole-2-carboxaldehyde (IC)
79 (Galloway et al., 2009), which absorbs light at UV wavelengths ($\lambda < 330$ nm) (Maxut et al., 2015).
80 Other imidazole-type compounds and light-absorbing products are formed in minor amounts but
81 can nonetheless impact optical and radiative properties of SOAs (Sareen et al., 2010; Trainic et
82 al., 2011). Photochemical reactions by these species are not typically accounted for in models yet,
83 but have a possible role for SOA formation and aerosol aging mechanisms (Sumner et al., 2014).
84 Photosensitizers are light absorbing compounds that absorb and convert the energy of photons into
85 chemical energy that can facilitate reactions, e.g., at surfaces or within aerosols (George et al.,
86 2015). For example, aerosol seeds containing humic acid or 4-(benzoyl)benzoic acid (4-BBA),
87 two other known photosensitizers, can induce the reactive uptake of VOCs when exposed to light,
88 leading to secondary organic aerosol (SOA) formation (Monge et al., 2012). Aregahegn et al.



89 (2013) and Rossignol et al. (2014) suggested a mechanism for autophotocatalytic aerosol growth,
90 where radicals are produced from the reaction of an H-donor hydrocarbon species, in this case
91 limonene, and the triplet state of IC. Field measurements on fog water samples confirmed that
92 triplet excited states of organic compounds upon irradiation can oxidize model samples such as
93 syringol (a biomass burning phenol) and methyl jasmonate (a green leaf volatile), accounting for
94 30 – 90% of their loss (Kaur et al., 2014).

95 The existence of such photocatalytic cycles could be of atmospheric significance. Canonica et al.
96 (1995) suggested indeed that the initial carbonyl, triggering the photochemical properties, is
97 regenerated via a reaction with oxygen producing HO₂. To our knowledge, the production of such
98 radical side products was not investigated under atmospheric conditions previously. We therefore
99 report here on the HO₂ radical production from IC in the condensed-phase.

100

101 **2. Experimental Section**

102 A series of flow tube experiments were conducted to investigate the formation of gas-phase HO₂
103 radicals from IC photochemistry using two different CWFT reactors (Sect. 2.1). Section 2.2
104 describes aerosol flow tube experiments that in absence of other known radical sources confirm
105 that HO₂ production from aerosols can start photochemistry. All experiments were performed at
106 atmospheric pressure.

107 **2.1. Coated-wall flow tube experiments**

108 The CWFT experiments were designed to investigate the gas-phase production of HO₂ radicals
109 from a film containing IC and citric acid (CA) matrix as a function of UV light intensity, IC
110 concentration in the film, relative humidity (RH), and O₂ mixing ratio. Two similar experimental
111 setups were used as shown in Fig. 1. Some of the differences, not major, consist in the flow reactor
112 volume, surface area, flow rates, IC mass loading, NO mixing ratio, temperature inside the reactor
113 and the connected instrumentation.

114 **Setup 1.** Experiments were conducted in a photochemical flow-system equipped with a Duran
115 glass CWFT (0.40 cm inner radius, 45.2 and 40.0 cm length, inner surface = 113.6 and 100.4 cm²,
116 S/V = 5.00 cm⁻¹), which was housed in a double jacketed cell coupled to a re-circulating water
117 bath to control the temperature at 298 K; The setup is shown in Fig. 1A. A thin film of IC+CA was



118 deposited inside the tubular glass flow tube. The experimental procedure for the preparation of
119 the films is described in Sect. 2.1.2. The system consisted of seven ultraviolet lamps (UV-A range,
120 Philips Cleo Effect 22 W: 300-420 nm, 41 cm, 2.6 cm o.d.) surrounding the flow tube in a circular
121 arrangement of 10 cm in diameter.

122 **Setup 2.** The second CWFT (CWFT 0.60 cm inner radius, 50 cm length, inner surface 188.5 cm²,
123 S/V = 3.33 cm⁻¹) reactor had a glass jacket to allow water to circulate and maintain temperature
124 control inside the tube at 292 K. The coated-wall tubes were snugly fit into the CWFT as inserts.
125 The CWFT was surrounded by the same seven fluorescent lamps as in Setup 1. The light passed
126 through different circulating water cooling jackets for both setups, thus providing a different light
127 path for each setup.

128 **Setup 1 and 2.** The actinic flux in the flow tube reactor, $F_{FT}(\lambda)$, was measured by actinometry of
129 NO₂ (see Supplement for description of J_{NO_2} measurements), independently for both setups. The
130 flows of N₂, O₂, air and NO were set by mass flow controllers. The RH was set by a humidifier
131 placed after the admission of N₂ and O₂ gases but before the admission of NO or NO₂ (see Fig. 1),
132 in which the carrier gas bubbles through liquid water at a given temperature. The humidifier could
133 also be by-passed to set a RH of near zero. A typical measurement sequence is described in Sect.
134 2.1.2.

135 The J_{NO_2} was measured for both Setup 1 and 2 using NO₂ actinometry. The J_{NO_2} with seven lamps
136 was found to be $2 \times 10^{-2} \text{ s}^{-1}$ for Setup 1 and $1 \times 10^{-2} \text{ s}^{-1}$ for Setup 2 (see Fig. S2 for Setup 1, and
137 Supplemental Information text for both Setups). These values were compared to direct irradiance
138 measurements in the flow tube and thus normalized (see Sect. 3.1.1).

139

140 **2.1.1. Flow tube instrumentation**

141 The following gas-phase products exiting the flow tube were measured by three different
142 instruments: NO₂ by the University of Colorado Light Emitting Diode Cavity-Enhanced
143 Differential Optical Absorption Spectroscopy (LED-CE-DOAS) instrument (Thalman and
144 Volkamer, 2010), HONO by a Long Path Absorption Photometer (LOPAP, QuMA GmbH,
145 Heland, J., 2001; Kleffmann et al., 2002), and NO by a chemiluminescence analyzer (Ecophysics
146 CLD 77 AM, also used for NO₂ in Setup 2). HO₂ radicals were indirectly measured by detecting



147 NO₂ with the LED-CE-DOAS (Setup 1) and by the loss of NO with the chemiluminescence
148 detector (Setup 2). The latter was preceded by a molybdenum converter to transform HONO and
149 NO₂ to NO, and by an alkaline trap for HONO. Both, trap and converter, had a bypass to allow
150 sequential measurements and thereby obtaining the concentration of NO₂ and HONO separately.
151 HONO was measured by the LOPAP during some selected experiments (Kleffmann et al., 2002,
152 2006).

153 **LED-CE-DOAS**

154 The LED-CE-DOAS instrument (Thalman and Volkamer, 2010) detects NO₂ absorption at blue
155 wavelengths. A high power blue LED light source (420–490 nm) is coupled to a confocal high
156 finesse optical cavity consisting of two highly reflective mirrors ($R = 0.999956$) peaking at 460
157 nm that are placed about 87.5 cm apart (sample path length of 74 cm). The absorption path length
158 depends on wavelength, and was about ~11 km near peak reflectivity here. A purge flow of dry
159 nitrogen gas is added to keep the mirrors clean. The light exiting the cavity is projected onto a
160 quartz optical fiber coupled to a Princeton Instruments Acton SP2156 Czerny-Turner imaging
161 spectrometer with a PIXIS 400B CCD detector. The mirror reflectivity was calculated by flowing
162 helium and nitrogen gas, exploiting the difference in the Rayleigh scattering cross sections of both
163 gases as described in Thalman et al. (2014). The gas exiting the flow tube was directly injected
164 into the CE-DOAS cavity, and spectra were recorded every 60 seconds, and stored on a computer.
165 For analysis we use BBCEAS fitting at NO₂ concentrations exceeding few ppbv (Washenfelder et
166 al., 2008) and DOAS least squares fitting methods at lower concentrations (Thalman et al., 2015).
167 The mirror alignment was monitored online as part of every spectrum by observing the slant
168 column density of oxygen collision complexes, O₂-O₂ (O₄) (Thalman and Volkamer, 2010, 2013).
169 The following reference spectra were taken from the literature: NO₂ (Vandaele et al., 2002) and
170 O₂-O₂ collision complexes (Thalman and Volkamer, 2013b). The detection limit for NO₂ was 50-
171 100 pptv.

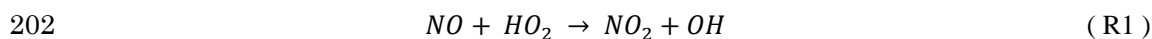
172 **2.1.2. Experimental conditions**

173 The IC+CA solutions were prepared by adding IC into a 1 M CA solution in 18 MΩ ultra-pure
174 water to achieve IC to CA molecular ratios between 0.026 to 0.127 in the film. The bulk solutions
175 for both Setup were prepared by weighing out 384-400 mg of CA in 2 mL of water and adding 4-
176 20 mg of IC to the solution. The solutions for both setups were freshly prepared for each



177 experiment and the masses in the film were calculated at 50% RH from the CA hygroscopic growth
178 factors reported by Zardini et al., 2008 for both setups (for Setup 1: 5-18 mg of IC and 44 mg of
179 CA, for Setup 2: 1-5 mg of IC and 77 mg of CA). The range of concentrations in the films was
180 between 0.148 – 0.671 M.

181 The IC+CA solution coatings were produced by depositing 220-250 μL (Setup 1) and 400 μL
182 (Setup 2) of the desired solution in a Duran glass tube, which was then dispersed into a thin and
183 viscous film. The film was dried with a gentle N_2 stream humidified to a RH similar to the
184 experimental RH and room temperature. The film was rolled and turned upside down to deposit a
185 homogenous film throughout the entire inner surface of the flow tube. The homogeneity of the
186 film was confirmed by visual inspection. If a bright clear homogenous amorphous film from the
187 super-cooled solution was not observed, the film was discarded (e.g. observation of a turbid and
188 cracked crystallized appearance). The carrier gas flows consisted of premixed dry N_2 and O_2 (a
189 ratio of 4.5/1 in Setup 1 and a ratio of 2 in Setup 2), and NO controlled by mass flow controllers.
190 The total flow rates were: 500 mL/min for Setup 1 and 1500 mL/min for Setup 2. In Setup 1, a
191 dilution flow of 1000 mL/min was added at the end of the flow tube for a total of 1500 mL/min
192 during experiments when HONO was measured along with NO_2 . All experiments were conducted
193 at ambient pressure, leading to gas residence times of 2.1 – 2.4 s (depending on flow tube volume,
194 for both setups) under laminar flow conditions. The O_2 flow rate was varied between 0-110
195 mL/min to observe the dependence of O_2 while keeping the total flow rate constant. A ratio of
196 4.5:1 of N_2 : O_2 was maintained if any of the other gas flows were changed (e.g. NO, and/or NO_2)
197 for Setup 1. For Setup 2, a ratio of 2:1 of N_2 : O_2 was also maintained, except for the O_2
198 concentration dependence studies. The RH was kept constant at 50% RH during most experiments,
199 and varied between 10-60% RH to study humidity effects of the HO_2 radical production. The
200 concentration of NO was ~ 1 ppmv (Setup 1) and varied between 100 and 500 ppbv (Setup 2).
201 Scavenging of HO_2 was achieved by the following reaction:



203 The lifetime of HO_2 is about 5 ms when 2.5×10^{13} molecules cm^{-3} of NO are present (Setup 1),
204 which assures efficient conversion of HO_2 molecules into NO_2 ($k = 8.0 \times 10^{-12}$ cm^3 molecule $^{-1}$ s $^{-1}$
205 at 298 K, Sander et al., 2011). As shown in Fig. S1, 500 ppbv NO, the concentration used in Setup
206 2, was sufficient to efficiently convert HO_2 into NO_2 , see Sect. 3.1.1. The lifetime of gas phase



207 HO₂ with respect to loss to the organic film is about 0.1 s, based on a similar formula shown in
 208 Equation S3, where $\gamma = 10^{-3}$ (upper limit by Lakey et al., 2015). Note that in view of the essentially
 209 diffusion controlled loss of HO₂ to the CWFT and tubing walls, the chosen scheme for determining
 210 the production of HO₂ radicals from the films by fast scavenging with NO is superior to a more
 211 selective detection method, e.g. LIF, which would require passing the HO₂ radicals into a separate
 212 setup with substantial losses. For selective experiments, the films were exposed to UV irradiation
 213 for over six hours which showed a minor change in the decrease of NO₂ concluding the stability
 214 of the reactivity of the films.

215 2.1.3. *J_{IC}* calculations

216 The absorption cross section of IC and the calculated photolysis rate are shown in Fig. S3. The
 217 photolysis frequencies of IC were calculated using a similar procedure as described in
 218 Schwarzenbach et al. (2002). The spectral irradiance in the flow tube system was interpolated to
 219 the surface area of the flow tube to calculate the spectral photon flux density and the absorbed
 220 photon flux:

$$221 \quad F_a^{IC} = \int_{300}^{420} F \times [1 - 10^{-\sigma_{IC}(\lambda) \times b \times C_{IC}}] d\lambda, \quad \text{where } F = \frac{F_{FT}(\lambda) \times SA}{N_a \times V_{film}}, \quad (1)$$

222 Where F_a^{IC} is the mean absorbed photon flux in Ein L⁻¹ s⁻¹ nm⁻¹ (1 Ein = 3.0 × 10⁵ J per mole of
 223 photons at 400 nm), F is the spectral flux density that reaches the film in the flow tube in moles L⁻¹
 224 s⁻¹ nm⁻¹, b is the optical path length taken as the thickness of the film and C_{IC} is the concentration
 225 of IC in the film, and σ_{IC} is the IC absorption cross section. The absorption spectrum of IC in
 226 water was based on the measurements by Kampf et al. (2012), and re-normalized to the peak value
 227 of 10205 ± 2400 M⁻¹ cm⁻¹ at 284 nm (Maxut et al., 2015). V_{film} is the volume of the film calculated
 228 from the deposited mass of CA and the hygroscopic growth factors of CA (Zardini et al., 2008),
 229 SA is the surface area of the flow tube of the film, taken as the geometric area of the inner surface
 230 area of the flow tube in cm², N_a is Avogadro's number in molecules mole⁻¹. The IC photoexcitation
 231 rate J_{IC} was about 1.0 × 10⁻³ s⁻¹ (upper limit).

232 We have also attempted to calculate an effective quantum yield for the formation of gas-phase
 233 HO₂ radicals (ϕ_{HO_2}):

$$234 \quad P_{HO_2} = \frac{[NO_2] \times flow}{N_a \times V_{film}} \quad \phi_{HO_2} = \frac{P_{HO_2}}{F_a^{IC}} \quad (2)$$



235 Where P_{HO_2} is the HO_2 production rate in $\text{mol L}^{-1} \text{s}^{-1}$, F_a^{IC} is the calculated mean absorbed photon
236 flux by IC (Eq. 1), $[NO_2]$ is the gas-phase concentration of NO_2 in molecules cm^{-3} assuming a 1:1
237 ratio to HO_2 conversion, $flow$ is the volumetric gas flow at the temperature in the CWTF and
238 atmospheric pressure in $\text{cm}^3 \text{s}^{-1}$, and V_{film} is in L.

239 2.2. Aerosol flow-reactor experiments

240 A detailed description of the aerosol flow tube (AFT) is reported elsewhere (Monge et al., 2012;
241 Aregahegn et al., 2013), therefore, only some principles are recalled below. The SOA experiments
242 were conducted in a horizontal, cylindrical, Pyrex, aerosol flow reactor (13 cm i. d., 152 cm length)
243 surrounded by seven UV lamps (Philips CLEO, 80W) with a continuous emission spectrum
244 ranging from 300-420 nm (total irradiance of 3.31×10^{16} photons $\text{cm}^{-2} \text{s}^{-1}$). The flow reactor
245 consisted of Teflon stoppers and different flow controllers that maintained the gas/aerosol/UV
246 irradiation contact time between 20-50 minutes. This flow reactor also consisted of an outer jacket
247 that controlled the temperature at 293 ± 2 K by water circulation using a thermostat (Model Huber
248 CC 405).

249 Seed aerosols (50 nm) were produced by nebulizing a solution (at pH 6) containing ammonium
250 sulfate (AS, 0.95 mM) and IC (1.3 mM), size selected by a DMA, and exposed to gas-phase
251 limonene (500 ppbv) in the aerosol flow reactor. The typical aerosol mass loading in the reactor
252 was $2\text{-}3 \mu\text{g cm}^{-3}$, corresponding to ~ 15000 particles cm^{-3} with a starting diameter of 50 nm. As
253 shown by Aregahegn et al. (in 2013), limonene is an efficient H-donor VOC that forms SOA via
254 reactive uptake to IC containing seed aerosol. Due to the excess of limonene, and low seed aerosol
255 surface are the consumption of limonene was below the detection limit. The aerosol growth was
256 measured by means of an Ultrafine Condensation Particle Counter (UCPC) and a Scanning
257 Mobility Particle Sizer Spectrometer (SMPS; both TSI), and similarly to the CWFT experiment, a
258 flow of gaseous NO (from a 1 ppmv cylinder, Linde) was added to the carrier gas, and its
259 conversion to NO_2 monitored by chemiluminescence detector with a detection limit of 0.05 ppbv
260 (ECO PHYSICS CLD 88). Due to the long residence time, the NO_2 concentration is affected by
261 its photolysis in the AFT. As discussed below, P_{HO_2} was calculated, in this case, from the growth
262 of the particle diameter measured at the exit of the flow tube; the assumption is that growth was
263 due to reactive uptake of limonene only, and that each limonene forms one HO_2 radical. At 30
264 ppbv NO, the HO_2 radical lifetime is around 2 sec.



265 **2.2.1. Experimental conditions**

266 The total flow rate in the aerosol flow reactor was between 400 – 1000 ml/min, ensuring laminar
267 flow conditions. The RH was varied between 0 – 50%. The RH of particles in the flow reactor
268 was controlled by saturating the carrier gas via a bubbler containing ultra-pure water (Milli Q, 18
269 Mohm). The RH in the flow reactor system was varied by changing the gas flow rates to the
270 bubbler and the temperature of the circulating water jacket of the bubbler. The RH was measured
271 with a humidity sensor (Meltec UFT 75-AT, Germany) at the exit of the flow reactor. The
272 concentrations for the flow tube experiments were the following: 30 ppbv of NO and 500 ppbv of
273 limonene.

274 **2.3. Chemicals**

275 The following chemicals were used without further purification for CWFT studies: IC (97%,
276 Sigma Aldrich), and CA (Sigma Aldrich). For Setup 1, the Duran glass tubes were soaked in a
277 deconex® cleaning solution overnight, the next day they were rinsed with 18 MΩ water (Milli Q
278 Element system). These flow tubes were etched with a 5% hydrofluoric acid solution after the
279 washing procedure and again rinsed with water before any experimental use. The Duran flow
280 tubes for Setup 2 were not initially etched with any acid but stored in a NaOH solution after
281 washing and lastly rinsed with water; Setup 2 later confirmed that the treatment of flow tube with
282 acids affects P_{HO_2} by rinsing with HCl and etching with HF solutions.

283 For the aerosol flow-reactor experiments gas-phase limonene was generated from commercially
284 available limonene (Aldrich, 97%) by means of a permeation tube. The following chemicals were
285 used without further purification: IC (97%, Sigma Aldrich) and succinic acid (Sigma Aldrich,
286 $\geq 99.5\%$); 4-benzoylbenzoic acid (4-BBA, Aldrich 99%) and adipic acid (AA, Aldrich, $\geq 99.5\%$)
287 were used to expand the CWFT studies to other photosensitizers.

288

289 **3. Results and Discussion**

290 **3.1. Coated-wall flow tube**

291 The following results represent the light dependent formation of HO_2 indirectly from
292 measurements of NO_2 production and NO loss, measured with setup 1 and 2, respectively. Figure



293 2 shows a time series of NO₂ measured with setup 1 as a function of UV-A light, which confirms
294 the light dependent radical production. This particular film had an IC/CA ratio of 0.026 (0.148M
295 IC and 5.77M CA in the film). An evident increase of NO₂ is observed upon UV irradiation,
296 directly reflecting the light mediated release of HO₂, as shown in reaction (R1). The NO₂ signal
297 decrease over time with all seven lamps was a common feature observed in all films; this could be
298 due to HO₂ sinks in the film increasing with time, thus, the system only slowly evolves into a
299 steady state. A small amount of NO₂ (0.5-1.5 ppbv) was observed during experiments that used
300 only CA in absence of IC; therefore, the data in Fig. 2 and all data reported below have been
301 corrected for this NO₂ background, measured routinely in between experiments. Figure 2 also
302 indicates a strong correlation with irradiance, which is further discussed in the context of Fig. 4.
303 Each data point was measured from a freshly prepared coated film in the flow tube. The
304 uncertainty for experiments was based on the standard deviation of *n*, the number of experiments.
305 The total uncertainty was ± 6-27% (propagated error for normalization was ± 7-29%) for the IC
306 mass loading experiments in Setup 1 and up to a factor of two for the light dependence
307 experiments. The uncertainty in Setup 2 was 10-50%. As discussed earlier, the lifetime of HO₂ in
308 the system was about three orders of magnitude less than the residence time in the flow tube,
309 therefore suggesting that most, if not all, reacted with NO to produce the observed NO₂ (R1).
310 Theoretically, the system was clean of other oxidants such as O₃ (and thus NO₃). The uptake of
311 NO₂ in the film was very small to further produce any nitrate radicals, and the photolysis of NO₂
312 in the experiments to produce O₃ was insignificant (< 1%). The recombination of NO and O₃
313 contributes a negligible (<0.1%) NO₂ source under our experimental conditions. RO₂ generation
314 from the reaction between CA and OH from HONO photolysis was also ruled out since it is
315 approximated to account for only 1% of the NO₂ production if we assume every OH from the
316 photolysis reacts with CA. To our knowledge, the direct photolysis of CA to produce any RO₂
317 radicals has not been observed. Therefore, we believe that HO₂ is the essential oxidant for NO
318 and refer to the measured NO₂ as HO₂ formation.

319 Figure 3 shows that the HO₂ production fluxes, in molecules cm⁻² min⁻¹, increased with IC mass
320 loading. The CA concentration was kept constant, and results are shown as the product between
321 [IC] × [CA], since we expect that the production rate of HO₂ is proportional to the concentration
322 of IC, at constant illumination, and that of the potential H-donor, CA. For Setup 1, the HO₂ fluxes
323 were measured as NO₂ mixing ratios, and calculated using the following equation:



$$324 \quad \text{Fluxes}_{\text{HO}_2} = \frac{[\text{NO}_2] \times \text{flow}}{SA} \quad (3)$$

325 the description of these parameters have been previously explained (see Sect. 2.1.3). For Setup 2,
 326 the HO₂ flux was calculated similarly, but only about half of the observed NO was considered to
 327 account for the loss of NO via the reaction with OH (see reaction in Supplement R1), meaning that
 328 for each HO₂ scavenged two NO molecules were lost. In Figure 3, the data from Setup 1 are
 329 represented by the black squares and the data from Setup 2 are represented by the gray circles.
 330 Setup 1 measurements were taken at about ~50% RH and at room temperature. Setup 2
 331 measurements were taken at 45% RH and at 292 K. Temperature has an effect on the observed
 332 gas-phase HO₂ release from the film and thus needs to be accounted for, which is not accounted
 333 for in Fig. 3 but it is described in detail in Sect. 3.1.1.

334 Figure 4 shows that the HO₂ production exhibited a linear dependence on the actinic flux for
 335 various [IC] × [CA] molar products. From Sect. 2.1.3, we estimated an experimental ϕ_{HO_2} of
 336 about 6×10^{-5} , reflecting other probable, unknown quenching processes in our system. Figure 4
 337 also shows the formation of HONO from three different IC mass loadings. In all three cases the
 338 HONO:NO₂ ratio is < 1, confirming HO₂ as a primary product and OH as a secondary product.
 339 Figure 5 shows the dependence of HO₂ production observed via the loss of NO (Setup 2) on
 340 relative humidity (0 – 65%). Water partial pressure is an important parameter in the atmosphere
 341 and it seems to also have an important effect on the photochemical reactions studied here. At RH
 342 below ~10%, and at high RH above ~55%, the yield of HO₂ radicals decreases. The maximum
 343 HO₂ radical production is observed at moderate RH (20 – 55%). This is probably due to a
 344 combination of factors. In particular, at low RH the film may become more viscous reducing
 345 mobility, and thus the energy transfer within the film. This may decrease the HO₂ yield as shown
 346 in Fig. 5. The reduced diffusivity of HO₂ may also increase the residence time in the film and
 347 facilitate the self-reaction in the bulk phase: The diffusivity of H₂O in citric acid is in the range of
 348 $10^{-7} - 10^{-8} \text{ cm}^2\text{s}^{-1}$ at 50% RH. If the HO₂ diffusivity is between a factor of 10 and 100 lower than
 349 that of H₂O due to its larger size, $10^{-9} \text{ cm}^2\text{s}^{-1}$, the first order loss rate coefficient for diffusion out
 350 of the film, D/δ^2 , δ denoting the film thickness ($4 \times 10^{-4} \text{ cm}$), becomes about $k_D = 10^{-2} \text{ s}^{-1}$. From the
 351 observed F_{HO_2} , the steady state concentration is then about $F_{\text{HO}_2}/k_D/\delta = 4 \times 10^{16} \text{ cm}^{-3} = 10^{-7} \text{ M}$. The
 352 loss rate coefficient due to HO₂ self-reaction in the condensed phase ($7.8 \times 10^5 \text{ M}^{-1} \text{ s}^{-1}$) at this
 353 concentration would become nearly 0.1 s^{-1} , somewhat higher than that for diffusional loss. Of



354 course these estimates carry a high uncertainty, but indicate that at lower humidity diffusivity gets
355 low enough to effectively reduce the diffusional loss of HO₂ to the gas phase and favor its loss by
356 self-reaction in the condensed phase. The potential presence of condensed phase sinks, such as
357 RO₂, formed from secondary chemistry of oxidized citric acid may add to this uncertainty. At
358 high RH (> 55%), the amount of water associated with CA dilutes the reactants, and quenching of
359 the excited IC triplet states gains in relative importance, consistent with findings in other studies
360 (Stemmler et al., 2006, 2007; Jammoul et al., 2008). The RH effect can decrease the HO₂
361 production by a factor of 3, compared to the plateau of maximum HO₂ production between 20 –
362 55% RH.

363 Figure 6 shows the dependence of the HO₂ production based on the observed NO loss on the O₂
364 mixing ratio (Setup 2). The HO₂ production varied by about 20% over the range of conditions
365 investigated. A marginal decrease below 15% O₂ appears to be significant compared to the
366 maximum HO₂ production at ~40% O₂, indicating that O₂ is needed for HO₂ formation. Sufficient
367 O₂ dissolves in the aqueous phase to produce HO₂ radicals efficiently at atmospheric O₂ mixing
368 ratios. Above 55% O₂ the HO₂ production decreased, which is probably due to quenching of
369 excited IC triplet states by O₂. Our results are qualitatively consistent with the observations of
370 decreasing aerosol growth at high O₂ in the autophotocatalytic aerosol growth described in
371 Aregahegn et al. (2013).

372 In order to test the possibility for excited IC triplet states to react with NO₂ at the surface of the
373 film, experiments were conducted with NO₂. While we did observe that the uptake of NO₂ on
374 irradiated surfaces scaled with light intensity (see Fig. S4) the reactive uptake coefficient of NO₂
375 to produce HONO at the surface is rather small (< 2.5 × 10⁻⁷), corresponding to a *k_w* of 10⁻³ s⁻¹ and
376 thus neither a significant loss of NO₂ nor a significant source of HONO. The primary fate of the
377 nitrogen-containing aromatic alkoxy IC radical under atmospheric conditions is reaction with O₂.
378 However, we have not tested alternative quenching reactions of the triplet state, or other pathways
379 of the reduced ketyl radical that do not result into formation of HONO.

380 3.1.1 Comparison of data sets

381 The experimental conditions probed differ in the actinic flux, NO concentration, temperature, and
382 acidity. Here, we use the dependencies established in Sect. 3.1 to compare results from both setups.
383 The data from Setup 2 were normalized to conditions of Setup 1. The difference in *J_{NO2}*



384 corresponds to multiplying results from Setup 2 with a factor of 2.0 ± 0.1 . HO₂ was measured
385 indirectly by reacting it with NO, and Fig. S1 indicates the minimum NO concentration needed to
386 efficiently scavenge all gas-phase HO₂ is ~460 ppbv of NO, indicating efficient conversion for
387 Setup 1, and a conversion efficiency of ~0.6 for Setup 2. The data from Setup 2 were multiplied
388 by 1.66 ± 0.10 to normalize for the NO conversion efficiency (Fig. S1), and by an additional factor
389 1.25 ± 0.10 to match temperatures. We observed some limited variability depending on whether
390 HF or HCl were used to clean the flow tube prior to experiments. A higher P_{HO₂} was observed
391 when cleaning with HF (Setup 1) compared to storing in NaOH and either rinsing with water or
392 HCl (Setup 2); this is accounted by multiplying data from Setup 2 with a factor of 1.25 ± 0.30 .
393 Notably, the error of the correction for the cleaning procedure that is propagated here is larger than
394 the correction factor. The effect of the pretreatment of the flow tubes was not systematically
395 studied, and thus remains a primary uncertainty in the comparison. No further correction was
396 applied for slight differences in RH. The overall correction factor amounts to 5.2 ± 1.4 , with the
397 error reflecting the propagated uncertainty. This explains most the difference in P_{HO₂} between both
398 setups. The normalized results agree within a factor of 2, which is a reasonably good agreement.

399 **3.1.2 Extension to other photosensitizers**

400 A limited number of experiments were performed using the CWFT approach, using 4-BBA as a
401 photosensitizer, in presence of 790 ppbv of gaseous limonene (a possible H-donor) and NO. The
402 organic thin film contained an organic acid matrix made of 4-BBA with/without adipic acid. Also
403 in this system a substantial conversion of NO into NO₂ was observed. That 4-BBA behaves similar
404 to the IC system demonstrates that the chemistry discussed above can occur on different excited
405 carbonyls. It is interesting to note that this photo-induced conversion, and HO₂ production, was
406 observed to be sustained over long times i.e., more than 15 h probably due to the catalytic nature
407 of the underlying chemical cycles. However, a fraction of the IC did get consumed by photolysis
408 reactions that do not form the excited triplet state (observed during overnight experiments). The
409 HO₂ flux for the 4-BBA system was estimated to be 2.77×10^{10} molecules cm⁻² min⁻¹ making the
410 same assumption that each HO₂ molecule reacts with NO to generate an NO₂ molecule. The
411 calculation is based on Eq. 3, where it depends on the concentration of NO₂ as well as the surface
412 area and residence time.

413 **3.2. Aerosol Flow Tube**



414 The aerosol flow tube experiments were conducted similarly to the study by Aregahegn et al.
415 (2013), i.e., who demonstrated that in the absence of NO and known gas phase oxidants, seed
416 particles containing IC can initiate SOA growth in presence of a gaseous H-donor (limonene).
417 Figure 7 shows the results from similar experiments when NO was added to the system. No
418 conversion of NO to NO₂ was observed prior to the injection of limonene into the flow tube. The
419 presence of a gaseous H-donor and light clearly initiated a series of photochemical processes,
420 leading to SOA growth and gaseous NO₂ production. However, the quantitative interpretation
421 of these experiments is not straightforward due to efficient radical cycling in the
422 VOC/NO_x/light photochemical system, and the lack of a blank experiment that did not contain
423 IC as part of the seed particles. Limitations arise from the much longer residence time, which
424 allows NO₂ to be significantly photolyzed. The J_{NO_2} was estimated as $\sim 6.75 \times 10^{-3} \text{ s}^{-1}$, and
425 corresponds to a photolysis lifetime of 2.5 minutes, which is smaller than the actual residence
426 time in the flow tube (~ 40 mins). Secondary chemistry can lead, among others, to ozone
427 production (O₃ lifetime at 500 ppbv limonene is ~ 7 min), and secondary OH radical formation
428 from the ozonolysis of limonene. Notably, NO_x is not consumed in Fig. 7. The overall effect
429 of this secondary chemistry is an increased SOA growth compared to an experiment without
430 added NO (Aregahegn et al., 2013). As a consequence, the NO₂ yield cannot be used directly
431 to assess P_{HO₂} in presence of NO.

432 However, in the absence of NO these secondary processes can largely be avoided, and are
433 reduced at a level where they cannot be identified (Aregahegn et al., 2013). Under such
434 conditions, the particle growth rates presumably carry information about the photosensitizer
435 cycling and subsequent HO₂ production. If we assume one molecule of limonene reacts to
436 produce one HO₂, the volume change of aerosols is proportional to the overall number of HO₂
437 produced. For example, a growth of 15,000 particles cm⁻³ from diameter 51.4 nm to 68.5 nm in 40
438 mins (residence time) is equal to P_{HO₂} of 1.67×10^{14} molecules cm⁻² min⁻¹. This should be
439 interpreted as an upper limit for the actual P_{HO₂}, because water uptake may also be
440 contributing to the volume growth. However, compared to the CWFT experiments the much
441 higher surface to volume ratio of nanoparticles is expected to enhance the chemical coupling
442 of a gas-phase H-donor and the excited IC triplet state at the aerosol surface. This is at least
443 in part deemed responsible for the two orders of magnitude higher P_{HO₂} in the aerosol flow



444 tube compared to the CWFT experiments. Notably, even if ϕ_{HO_2} in the aerosol flow tube was
445 two order of magnitude higher than in the CWFT, it is still significantly smaller than unity.

446 **Primary HO₂ formation from IC**

447 One of the main advantages of the CWFT is that it operates at much shorter residence time. From
448 Setup 1, we derive a P_{HO_2} of 1.76×10^{12} molecules $\text{cm}^{-2} \text{min}^{-1}$ for $IC/CA = 0.1$ and $J_{NO_2} = 8 \times 10^{-}$
449 $^3 \text{s}^{-1}$. This corresponds to 2.9×10^4 molecules $\text{cm}^{-3} \text{s}^{-1}$ once normalized by aerosol surface area
450 ($1.18 \times 10^{-6} \text{cm}^2 \text{cm}^{-3}$), and J_{NO_2} in the aerosol flow tube. Such a primary radical flux is equivalent
451 to the OH radical production rate resulting from photolysis of ~ 1 pptv of HONO in the aerosol
452 flow tube. Conversely, a P_{HO_2} of 1.67×10^{14} molecules $\text{cm}^{-2} \text{min}^{-1}$ is equivalent to the OH radical
453 production rate from ~ 100 pptv HONO in the aerosol flow tube. We conclude that seed particles
454 containing IC contribute significantly (equivalent to 1-100 pptv HONO) to the primary HO_x radical
455 production rate in the aerosol flow tube experiments in the presence of NO (Fig. 7). Primary HO₂
456 radicals formed from IC containing seed particles react rapidly with NO to form OH radicals under
457 the conditions shown in Figure 7. The H-donor species is further expected to form primary RO₂
458 radicals. These primary HO₂ and RO₂ radicals add directly to the conversion of NO into NO₂, and
459 indirectly by driving secondary NO-to-NO₂ conversion from the RO₂/HO₂ radical chain. The
460 aerosol flow tube experiments thus qualitatively confirm the results obtained from macroscopic
461 surfaces, and highlight the potentially important role of surface-to-volume ratio and gaseous H-
462 donors to enhance the relevance of H-donor photochemistry as sources for HO_x/RO_x radicals and
463 SOA.

464 **3.3. Proposed mechanism**

465 A mechanism that can describe the results from the CWFT experiments is shown in Fig. 8. It
466 follows the mechanism first proposed by Canonica et al., in 1995. The primary product in our
467 system is the HO₂ radical, which forms from the reaction between a nitrogen-containing aromatic
468 alkoxy IC radical and a ground state oxygen molecule, recycling the IC molecule. The aromatic
469 alkoxy radicals form from the excited triplet state of IC via transfer of an H atom from an H-donor
470 (in our case likely to be CA, or the CA/H₂O matrix). While a fraction of the IC will get consumed
471 by photolysis reactions that do not form the excited triplet state (see Sect 3.1.2.), IC is also
472 continuously produced from multiphase reactions, e.g., of glyoxal (Yu et al., 2011; Kampf et al.,
473 2012; Maxut et al., 2015). Another conclusion is that OH is a secondary product. If OH was a first



474 generation product we would have expected HONO:NO₂ ratios larger than 1:1. A smaller ratio
475 was observed, as shown in Fig. 4, indicating that there was no direct evidence for primary
476 formation of OH radicals. Interestingly, the H-donor species becomes activated as a result of H-
477 abstraction, and can react further to produce organic peroxy radicals, as evidenced by the aerosol
478 flow tube results.

479

480 **4. Atmospheric relevance**

481 The atmospheric relevance of our findings consists of the possible effect of heterogeneous radical
482 sources to modify atmospheric HO₂ radical concentrations, and facilitate aerosol growth and
483 ageing by adding a radical source within aerosol particles. The production of gas-phase HO₂ from
484 IC photosensitized heterogeneous chemistry is a possible source of gas-phase HO₂ radicals in
485 ambient air. In order to estimate the possible relevance for HO₂ radical concentrations in urban air,
486 we assume P_{HO₂} of 2×10^{12} molecules cm⁻² min⁻¹ (IC/CA = 0.1, Setup 1) as a lower limit, and 2
487 $\times 10^{14}$ molecules cm⁻² min⁻¹ (IC/AS = 0.1, aerosol flow tube) as an upper limit, and typical
488 conditions in Mexico City (i.e., $J_{NO_2} = 8 \times 10^{-3}$ s⁻¹ at noontime in Mexico City, aerosol surface
489 area = 15 cm² m⁻³; Volkamer et al., 2007). The normalized P_{HO₂} during noon time in Mexico City
490 ranges from 2×10^5 to 2×10^7 molecules cm⁻³ s⁻¹. This corresponds to a rate of new HO₂ radical
491 production of 4 to 400 pptv HONO around solar noon in Mexico City (Li et al., 2010), where other
492 radical sources produce about 5.9×10^7 molecules cm⁻³ s⁻¹ at solar noon (Volkamer et al., 2010).
493 The upper range value suggests that aerosol surfaces can be a significant source of gas-phase HO_x
494 in places like Mexico City. However, the IC molar ratios used here are likely an upper limit
495 compared to ambient aerosols, yet, in principle other brown carbon molecules (i.e. HULIS and/or
496 other imidazole derivatives) may form additional gas-phase HO₂. The heterogeneous HO₂ radical
497 source could further be relatively more important in unpolluted regions under biogenic influences,
498 where gas-phase radical production rates are lower. A more comprehensive characterization of the
499 heterogeneous HO₂ source effect on gas-phase HO₂ radical concentrations hence deserves further
500 investigation.

501 OH radical uptake from the gas-phase is a primary OH source in aerosols (Ervens and Volkamer,
502 2010). Assuming a gas-phase OH concentration of 10^6 molecules cm⁻³, 15 cm² m⁻³ aerosol surface



503 area, and γ_{OH} of unity, the rate of OH uptake is approximately 2.3×10^5 molecules $\text{cm}^{-3} \text{s}^{-1}$. The
504 above estimated P_{HO_2} is a result from H-transfer to form organic peroxy radicals which is
505 comparable to the rate of OH uptake. The two similar estimates of HO_x suggest that IC is a
506 significant source of radicals in the condensed phase of particles. This is a lower limit due to the
507 unknown radical losses of HO_x to the condensed phase, which hold potential to leverage the HO_x
508 source by up to a factor 10,000 if limited by the IC excitation rate. The unknown amount of HO_2
509 that remains in the condensed-phase is a further source of OH in the condensed-phase that can start
510 Fenton reactions (if iron is present) or other oxidizing pathways that can further age the aerosol.
511 These results show that IC, and other aromatic carbonyl photosensitizers, are likely a relevant
512 radical source in aerosol particles. Photo-induced radical generation in condensed phases is
513 currently not represented in atmospheric models that describe aerosol ageing, and warrant further
514 study.

515

516 5. Conclusion

517 Three different experimental setups consistently show that HO_2 radicals are produced from the
518 photochemistry of IC in a CA+ H_2O matrix and in seed aerosols containing ammonium sulfate (in
519 presence of a gas-phase H-donor, limonene). The linear correlations of P_{HO_2} (with $[\text{IC}]/[\text{CA}]$ and
520 irradiation) yielded maximum P_{HO_2} under atmospherically relevant irradiation, O_2 and RH, but
521 also revealed a complex role of film viscosity, and possibly acid effects. If the H-donor species is
522 in the condensed phase, significant amounts of HO_2 reach the gas-phase only for moderately high
523 RH (~25 – 55% RH) that facilitates H-transfer, and allows molecules (IC, HO_2) to move freely
524 towards the surface of the film. When the film was too dry this mobility is inhibited due to enhance
525 viscosity and significantly decreases the P_{HO_2} . At RH and O_2 higher than 55%, we observe a
526 decrease in P_{HO_2} probably due to dilution by water and competing quenching reactions in the film.
527 If the H-donor species is in the gas-phase, significant HO_2 production is also observed under dry
528 conditions. The primary fate of the $\text{IC}\cdot\text{OH}$ radical at the surface is reaction with O_2 to form HO_2 .
529 NO_2 reactions do not appear to form HONO at the surface. Our results suggest that the radical
530 source from photosensitizers such as IC can help jump-start photochemistry of VOCs. The effect
531 on the gas-phase HO_2 radical concentration increases for higher surface to volume ratio of aerosols,
532 and in the presence of gas-phase H-donors. The autophotocatalytic growth of aerosols containing



533 photosensitizers via H-donor chemistry is a SOA source also in the presence of NO, and adds
534 oxidative capacity inside aerosol particles. Further research on other types of H-donors and
535 photosensitizers is necessary to compare different P_{HO_2} and rates of aerosol growth from reactive
536 uptake of VOC that could potentially have a significant atmospheric relevance for SOA formation
537 and heterogeneous aerosol ageing.

538 **Author contributions**

539 M.A. and R.V. designed the experiments at PSI; C.G. and B.N. those at IRCELYON. L.G.P.,
540 P.C.A., and K.Z.A. conducted the measurements, analyzed data, and contributed equally to this
541 work. S.S.S., T.B.R. helped during the experiments, and all co-authors contributed to the data
542 interpretation. L.G.P. and R.V. prepared the manuscript with contributions from all co-authors.

543

544 **Acknowledgements**

545 This work was supported by the US National Science Foundation under awards ATM-847793 and
546 AGS-1452317. M.A. and C.G. appreciate the contribution by the EU project PEGASOS (EU-FP7
547 project under grant agreement no. 265307). M.A. appreciates the Swiss National Science
548 Foundation (grant 130179).

549 **References**

- 550 Aregahegn, K. Z., Nozière, B. and George, C.: Organic aerosol formation photo-enhanced by the
551 formation of secondary photosensitizers in aerosols, *Faraday Discuss.*, 165(0), 123–134,
552 doi:10.1039/C3FD00044C, 2013.
- 553 Atkinson, R., Baulch, D. L., Cox, R. A., Crowley, J. N., Hampson, R. F., Hynes, R. G., Jenkin,
554 M. E., Rossi, M. J. and Troe, J.: Evaluated kinetic and photochemical data for atmospheric
555 chemistry: Volume I - gas phase reactions of Ox, HOx, NOx and SOx species, *Atmos Chem*
556 *Phys.*, 4(6), 1461–1738, doi:10.5194/acp-4-1461-2004, 2004.
- 557 Badali, K. M., Zhou, S., Aljawhary, D., Antiñolo, M., Chen, W. J., Lok, A., Mungall, E., Wong,
558 J. P. S., Zhao, R. and Abbatt, J. P. D.: Formation of hydroxyl radicals from photolysis of
559 secondary organic aerosol material, *Atmos Chem Phys.*, 15(14), 7831–7840, doi:10.5194/acp-15-
560 7831-2015, 2015.
- 561 Calvert, J. G. and Pitts, J. N.: *Photochemistry*, Wiley, New York., 1966.
- 562 Canonica, S., Jans, U., Stemmler, K. and Hoigne, J.: Transformation Kinetics of Phenols in
563 Water: Photosensitization by Dissolved Natural Organic Material and Aromatic Ketones,
564 *Environ. Sci. Technol.*, 29(7), 1822–1831, doi:10.1021/es00007a020, 1995.
- 565 Deguillaume, L., Leriche, M., Desboeufs, K., Mailhot, G., George, C. and Chaumerliac, N.:
566 Transition metals in atmospheric liquid phases: sources, reactivity, and sensitive parameters,
567 *Chem. Rev.*, 105(9), 3388–3431, doi:10.1021/cr040649c, 2005.
- 568 Draper, W. M. and Crosby, D. G.: Photochemical generation of superoxide radical anion in
569 water, *J. Agric. Food Chem.*, 31(4), 734–737, doi:10.1021/jf00118a014, 1983.
- 570 Dupart, Y., King, S. M., Nekat, B., Nowak, A., Wiedensohler, A., Herrmann, H., David, G.,
571 Thomas, B., Miffre, A., Rairoux, P., D’Anna, B. and George, C.: Mineral dust photochemistry
572 induces nucleation events in the presence of SO₂, *Proc. Natl. Acad. Sci. U. S. A.*, 109(51),
573 20842–20847, doi:10.1073/pnas.1212297109, 2012.
- 574 Ervens, B., Gligorovski, S. and Herrmann, H.: Temperature-dependent rate constants for
575 hydroxyl radical reactions with organic compounds in aqueous solutions, *Phys. Chem. Chem.*
576 *Phys.*, 5(9), 1811–1824, doi:10.1039/b300072a, 2003.
- 577 Ervens, B., Turpin, B. J. and Weber, R. J.: Secondary organic aerosol formation in cloud droplets
578 and aqueous particles (aqSOA): a review of laboratory, field and model studies, *Atmos Chem*
579 *Phys.*, 11(21), 11069–11102, doi:10.5194/acp-11-11069-2011, 2011.
- 580 Faust, B. C.: Aquatic Photochemical Reactions in Atmospheric, Surface, and Marine Waters:
581 Influences on Oxidant Formation and Pollutant Degradation, in *Environmental Photochemistry*,
582 edited by D. P. Boule, pp. 101–122, Springer Berlin Heidelberg. [online] Available from:
583 http://link.springer.com/chapter/10.1007/978-3-540-69044-3_4 (Accessed 7 December 2015),
584 1999.



- 585 Fenton, H. J. H.: LXXIII. Oxidation of tartaric acid in presence of iron, *J. Chem. Soc. Trans.*, 65,
586 899, doi:10.1039/ct8946500899, 1894.
- 587 Galloway, M. M., Chhabra, P. S., Chan, A. W. H., Surratt, J. D., Flagan, R. C., Seinfeld, J. H.
588 and Keutsch, F. N.: Glyoxal uptake on ammonium sulphate seed aerosol: reaction products and
589 reversibility of uptake under dark and irradiated conditions, *Atmos Chem Phys*, 9(10), 3331–
590 3345, doi:10.5194/acp-9-3331-2009, 2009.
- 591 George, C., Strekowski, R. S., Kleffmann, J., Stemmler, K. and Ammann, M.: Photoenhanced
592 uptake of gaseous NO₂ on solid organic compounds: a photochemical source of HONO?,
593 *Faraday Discuss.*, 130, 195–210; discussion 241–264, 519–524, 2005.
- 594 George, C., Ammann, M., D’Anna, B., Donaldson, D. J. and Nizkorodov, S. A.: Heterogeneous
595 Photochemistry in the Atmosphere, *Chem. Rev.*, doi:10.1021/cr500648z, 2015.
- 596 Heland, J., J. K.: A new instrument to measure gaseous nitrous acid (HONO) in the atmosphere.,
597 *Environ. Sci. Amp Technol.*, 35(15), 3207–12, doi:10.1021/es000303t, 2001.
- 598 Jacob, D.: *Introduction to Atmospheric Chemistry*, Princeton University Press, Princeton, N.J.,
599 1999.
- 600 Jammoul, A., Gligorovski, S., George, C. and D’Anna, B.: Photosensitized Heterogeneous
601 Chemistry of Ozone on Organic Films, *J. Phys. Chem. A*, 112(6), 1268–1276,
602 doi:10.1021/jp074348t, 2008.
- 603 Kampf, C. J., Jakob, R. and Hoffmann, T.: Identification and characterization of aging products
604 in the glyoxal/ammonium sulfate system – implications for light-absorbing material in
605 atmospheric aerosols, *Atmos Chem Phys*, 12(14), 6323–6333, doi:10.5194/acp-12-6323-2012,
606 2012.
- 607 Kaur, R., Anastasio, C., Valsaraj, K. T., Vempati, H. S. and Vaitilingom, M.: Photoformation of
608 Triplet Excited States and Other Oxidants in Fog Waters and Their Impact on Fog Processing of
609 Organic Compounds, *AGU Fall Meet. Abstr.*, 53, 07, 2014.
- 610 Kleffmann, J., Heland, J., Kurtenbach, R., Lörzer, J. C. and Wiesen, P.: A new instrument
611 (LOPAP) for the detection of nitrous acid (HONO), *Environ. Sci. Pollut. Res.*, 9(4), 48–54,
612 2002.
- 613 Kleffmann, J., Wiesen, P. and Kern, C.: Intercomparison of the DOAS and LOPAP techniques
614 for the detection of nitrous acid, 2006.
- 615 Lakey, P. S. J., George, I. J., Whalley, L. K., Baeza-Romero, M. T. and Heard, D. E.:
616 Measurements of the HO₂ Uptake Coefficients onto Single Component Organic Aerosols,
617 *Environ. Sci. Technol.*, 49(8), 4878–4885, doi:10.1021/acs.est.5b00948, 2015.
- 618 Li, G., Lei, W., Zavala, M., Volkamer, R., Dusanter, S., Stevens, P. and Molina, L. T.: Impacts
619 of HONO sources on the photochemistry in Mexico City during the MCMA-2006/MILAGO
620 Campaign, *Atmos Chem Phys*, 10(14), 6551–6567, doi:10.5194/acp-10-6551-2010, 2010.



- 621 Maxut, A., Noziere, B., Fenet, B. and Mechakra, H.: Formation Mechanism and yield of small
622 Imidazoles from Reactions of Glyoxal with NH₄⁺ in water at neutral pH, *Phys. Chem. Chem.*
623 *Phys.*, doi:10.1039/C5CP03113C, 2015.
- 624 Monge, M. E., Rosenørn, T., Favez, O., Müller, M., Adler, G., Riziq, A. A., Rudich, Y.,
625 Herrmann, H., George, C. and D'Anna, B.: Alternative pathway for atmospheric particles
626 growth, *Proc. Natl. Acad. Sci.*, 109(18), 6840–6844, doi:10.1073/pnas.1120593109, 2012.
- 627 Monks, P. S.: Gas-phase radical chemistry in the troposphere, *Chem. Soc. Rev.*, 34(5), 376–395,
628 doi:10.1039/B307982C, 2005.
- 629 Nozière, B., Dziedzic, P. and Córdova, A.: Products and Kinetics of the Liquid-Phase Reaction
630 of Glyoxal Catalyzed by Ammonium Ions (NH₄⁺), *J. Phys. Chem. A*, 113(1), 231–237,
631 doi:10.1021/jp8078293, 2009.
- 632 Rossignol, S., Aregahegn, K. Z., Tinel, L., Fine, L., Nozière, B. and George, C.: Glyoxal induced
633 atmospheric photosensitized chemistry leading to organic aerosol growth, *Environ. Sci.*
634 *Technol.*, 48(6), 3218–3227, doi:10.1021/es405581g, 2014.
- 635 Sander, S. P., Abbatt, J., Barker, J. R., Burkholder, J. B., Friedl, R. R., Golden, D. M., Huie, R.
636 E., Kolb, C. E., Kurylo, M. J., Moortgat, G. K., Orkin, V. L. and Wine, P. H.: Chemical Kinetics
637 and Photochemical Data for Use in Atmospheric Studies, Evaluation No. 17, JPL Publ. 10-6, Jet
638 Propulsion Laboratory, Pasadena [online] Available from: <http://jpldataeval.jpl.nasa.gov>, 2011.
- 639 Sareen, N., Schwier, A. N., Shapiro, E. L., Mitroo, D. and McNeill, V. F.: Secondary organic
640 material formed by methylglyoxal in aqueous aerosol mimics, *Atmos Chem Phys*, 10(3), 997–
641 1016, doi:10.5194/acp-10-997-2010, 2010.
- 642 Schwarzenbach, R. P., Gschwend, P. M. and Imboden, D. M.: *Environmental Organic*
643 *Chemistry*, 2 edition., Wiley-Interscience, New York., 2002.
- 644 Shapiro, E. L., Szprengiel, J., Sareen, N., Jen, C. N., Giordano, M. R. and McNeill, V. F.: Light-
645 absorbing secondary organic material formed by glyoxal in aqueous aerosol mimics, *Atmos*
646 *Chem Phys*, 9(7), 2289–2300, doi:10.5194/acp-9-2289-2009, 2009.
- 647 Sheehy, P. M., Volkamer, R., Molina, L. T. and Molina, M. J.: Oxidative capacity of the Mexico
648 City atmosphere – Part 2: A ROx radical cycling perspective, *Atmos Chem Phys*, 10(14), 6993–
649 7008, doi:10.5194/acp-10-6993-2010, 2010.
- 650 Stemmler, K., Ammann, M., Donders, C., Kleffmann, J. and George, C.: Photosensitized
651 reduction of nitrogen dioxide on humic acid as a source of nitrous acid, *Nature*, 440(7081), 195–
652 198, doi:10.1038/nature04603, 2006.
- 653 Stemmler, K., Ammann, M., Elshorbany, Y., Kleffmann, J., Ndour, M., D'Anna, B., George, C.
654 and Bohn, B.: Light induced conversion of nitrogen dioxide into nitrous acid on submicron
655 humic acid aerosol, *Atmos Chem Phys*, 7, 4035–4064, 2007.



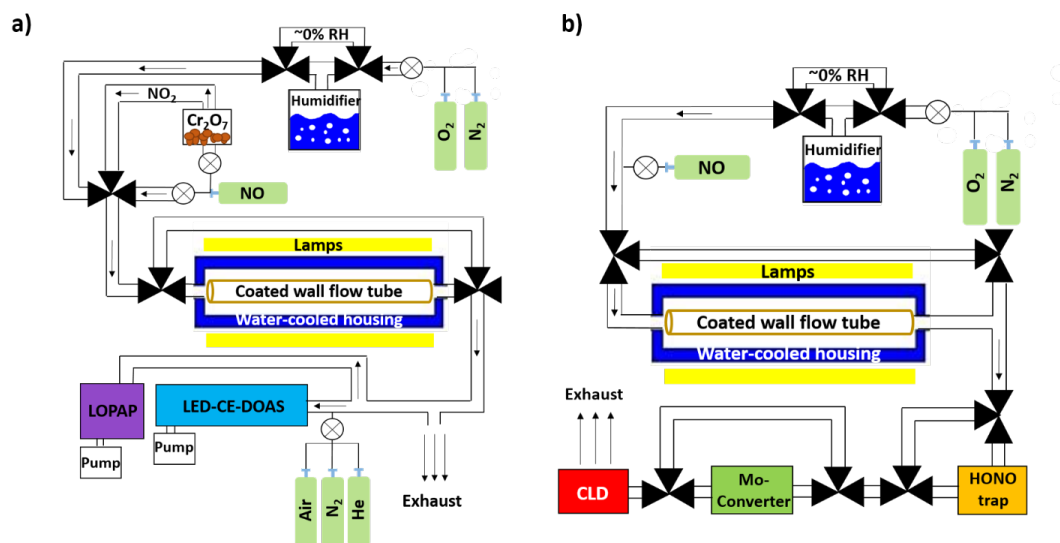
- 656 Sumner, A. J., Woo, J. L. and McNeill, V. F.: Model Analysis of Secondary Organic Aerosol
657 Formation by Glyoxal in Laboratory Studies: The Case for Photoenhanced Chemistry, Environ.
658 Sci. Technol., 48(20), 11919–11925, doi:10.1021/es502020j, 2014.
- 659 Thalman, R. and Volkamer, R.: Inherent calibration of a blue LED-CE-DOAS instrument to
660 measure iodine oxide, glyoxal, methyl glyoxal, nitrogen dioxide, water vapour and aerosol
661 extinction in open cavity mode, Atmos Meas Tech, 3(6), 1797–1814, doi:10.5194/amt-3-1797-
662 2010, 2010.
- 663 Thalman, R. and Volkamer, R.: Temperature dependent absorption cross-sections of O₂–O₂
664 collision pairs between 340 and 630 nm and at atmospherically relevant pressure, Phys. Chem.
665 Chem. Phys., 15(37), 15371–15381, doi:10.1039/C3CP50968K, 2013.
- 666 Thalman, R., Zarzana, K. J., Tolbert, M. A. and Volkamer, R.: Rayleigh scattering cross-section
667 measurements of nitrogen, argon, oxygen and air, J. Quant. Spectrosc. Radiat. Transf., 147, 171–
668 177, doi:10.1016/j.jqsrt.2014.05.030, 2014.
- 669 Thalman, R., Baeza-Romero, M. T., Ball, S. M., Borrás, E., Daniels, M. J. S., Goodall, I. C. A.,
670 Henry, S. B., Karl, T., Keutsch, F. N., Kim, S., Mak, J., Monks, P. S., Muñoz, A., Orlando, J.,
671 Peppe, S., Rickard, A. R., Ródenas, M., Sánchez, P., Seco, R., Su, L., Tyndall, G., Vázquez, M.,
672 Vera, T., Waxman, E. and Volkamer, R.: Instrument intercomparison of glyoxal, methyl glyoxal
673 and NO₂ under simulated atmospheric conditions, Atmos Meas Tech, 8(4), 1835–1862,
674 doi:10.5194/amt-8-1835-2015, 2015.
- 675 Trainic, M., Abo Riziq, A., Lavi, A., Flores, J. M. and Rudich, Y.: The optical, physical and
676 chemical properties of the products of glyoxal uptake on ammonium sulfate seed aerosols,
677 Atmos Chem Phys, 11(18), 9697–9707, doi:10.5194/acp-11-9697-2011, 2011.
- 678 Vandaele, A. C., Hermans, C., Fally, S., Carleer, M., Colin, R., Mérienne, M.-F., Jenouvrier, A.
679 and Coquart, B.: High-resolution Fourier transform measurement of the NO₂ visible and near-
680 infrared absorption cross sections: Temperature and pressure effects, J. Geophys. Res.
681 Atmospheres, 107(D18), 4348, doi:10.1029/2001JD000971, 2002.
- 682 Volkamer, R., San Martini, F., Molina, L. T., Salcedo, D., Jimenez, J. L. and Molina, M. J.: A
683 missing sink for gas-phase glyoxal in Mexico City: Formation of secondary organic aerosol,
684 Geophys. Res. Lett., 34(19), L19807, doi:10.1029/2007GL030752, 2007.
- 685 Volkamer, R., Sheehy, P., Molina, L. T. and Molina, M. J.: Oxidative capacity of the Mexico
686 City atmosphere – Part 1: A radical source perspective, Atmos Chem Phys, 10(14), 6969–6991,
687 doi:10.5194/acp-10-6969-2010, 2010.
- 688 Washenfelder, R. A., Langford, A. O., Fuchs, H. and Brown, S. S.: Measurement of glyoxal
689 using an incoherent broadband cavity enhanced absorption spectrometer, Atmos Chem Phys,
690 8(24), 7779–7793, doi:10.5194/acp-8-7779-2008, 2008.
- 691 Weller, C., Horn, S. and Herrmann, H.: Effects of Fe(III)-concentration, speciation, excitation-
692 wavelength and light intensity on the quantum yield of iron(III)-oxalato complex photolysis, J.
693 Photochem. Photobiol. Chem., 255, 41–49, doi:10.1016/j.jphotochem.2013.01.014, 2013a.



- 694 Weller, C., Horn, S. and Herrmann, H.: Photolysis of Fe(III) carboxylato complexes: Fe(II)
695 quantum yields and reaction mechanisms, *J. Photochem. Photobiol. Chem.*, 268, 24–36,
696 doi:10.1016/j.jphotochem.2013.06.022, 2013b.
- 697 Yi, J., Bahrini, C., Schoemaeker, C., Fittschen, C. and Choi, W.: Photocatalytic Decomposition
698 of H₂O₂ on Different TiO₂ Surfaces Along with the Concurrent Generation of HO₂ Radicals
699 Monitored Using Cavity Ring Down Spectroscopy, *J. Phys. Chem. C*, 116(18), 10090–10097,
700 doi:10.1021/jp301405e, 2012.
- 701 Yu, G., Bayer, A. R., Galloway, M. M., Korshavn, K. J., Fry, C. G. and Keutsch, F. N.: Glyoxal
702 in Aqueous Ammonium Sulfate Solutions: Products, Kinetics and Hydration Effects, *Environ.*
703 *Sci. Technol.*, 45(15), 6336–6342, doi:10.1021/es200989n, 2011.
- 704 Zardini, A. A., Sjogren, S., Marcolli, C., Krieger, U. K., Gysel, M., Weingartner, E.,
705 Baltensperger, U. and Peter, T.: A combined particle trap/HTDMA hygroscopicity study of
706 mixed inorganic/organic aerosol particles, *Atmos Chem Phys*, 8(18), 5589–5601,
707 doi:10.5194/acp-8-5589-2008, 2008.
- 708 Zellner, R., Exner, M. and Herrmann, H.: Absolute OH quantum yields in the laser photolysis of
709 nitrate, nitrite and dissolved H₂O₂ at 308 and 351 nm in the temperature range 278–353 K, *J.*
710 *Atmos. Chem.*, 10, 411–425, 1990.
- 711 Zhao, R., Lee, A. K. Y., Soong, R., Simpson, A. J. and Abbatt, J. P. D.: Formation of aqueous-
712 phase α -hydroxyhydroperoxides (α -HHP): potential atmospheric impacts, *Atmos Chem Phys*,
713 13(12), 5857–5872, doi:10.5194/acp-13-5857-2013, 2013.
- 714



715 **Figures**



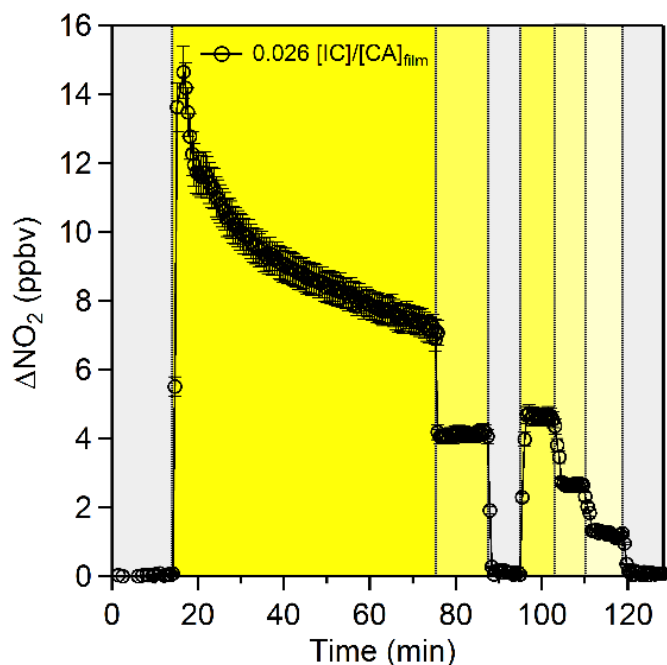
716

717 Figure 1. Sketch of the photochemical flow tube reactor setups at PSI for a) Setup 1 in 2013

718 measuring NO₂ generation and b) for Setup 2 in 2014 measuring NO loss.



719



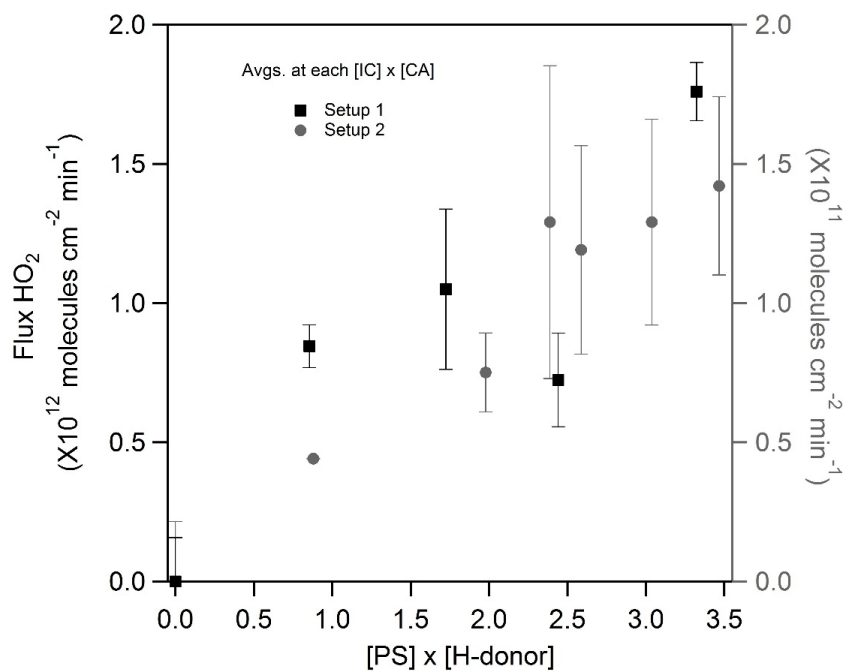
720

721

722 Figure 2. NO₂ profile for a 0.025M IC bulk solution, whose concentration increases to ~0.2 M of
723 IC in the film due to the citric acid hygroscopic properties. The gray shaded areas indicate
724 periods where NO was exposed in the dark. The yellow shaded areas indicates the period of
725 irradiation; the decrease in the intensity of yellow represents the decrease in irradiance ($2.26 \times$
726 10^{16} , 1.47×10^{16} , 1.14×10^{16} , and 3.94×10^{15} photons $\text{cm}^{-2} \text{s}^{-1}$, for seven, five, three and one
727 lamp, respectively). This timeseries clearly indicates the light dependence production of HO₂
728 radicals from the photosensitization of IC in a CA film.

729

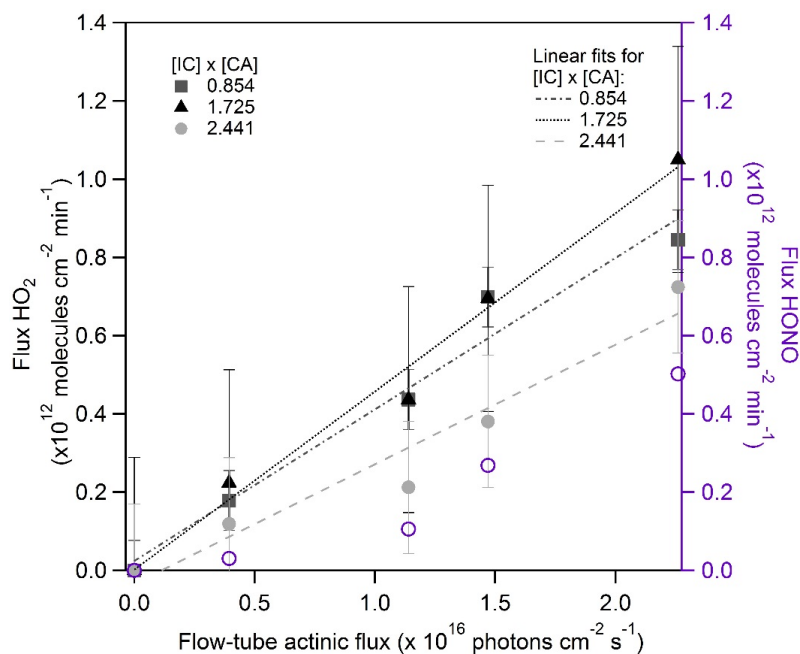
730



731

732 Figure 3. A linear correlation of HO₂ as a function of IC concentration. The left y-axis
733 represents the values for Setup 1, while the right y-axis represents the values for Setup 2, (an
734 order of magnitude difference for both scales). The Setup 2 data falls between a factor of 2 and 3
735 from Setup 1 after accounting for differences between Setup 1 and 2, see Sect. 3.1.1.

736



737

738

739 Figure 4. HO_2 fluxes (molecules cm^{-2} min^{-1}) as a function of actinic flux for a 300-420 nm range.

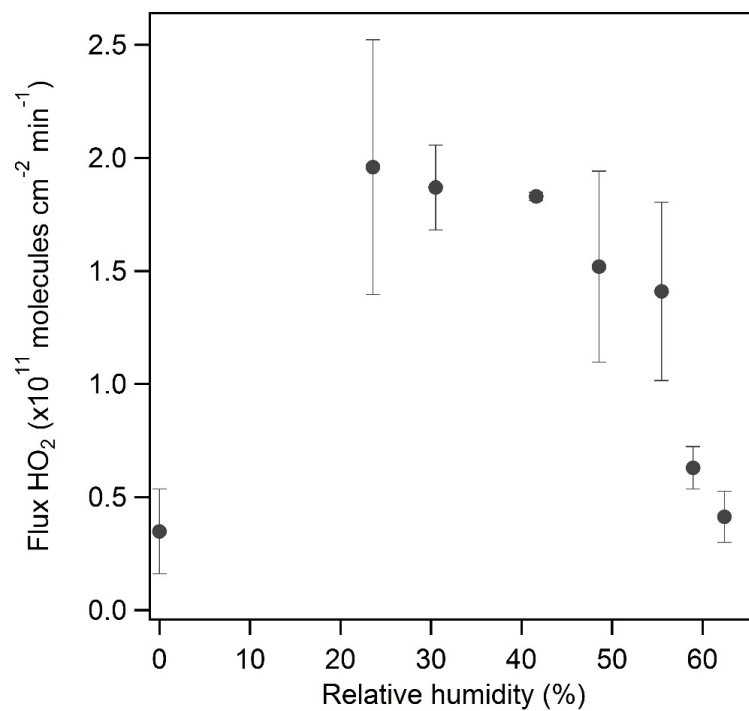
740 The data is plotted as a concentration product of $[\text{IC}] \times [\text{CA}]$ (shown in the legend) which shows

741 the photochemical reaction between IC and CA in H_2O matrix and gaseous NO. HONO for

742 2.441 ($[\text{IC}] \times [\text{CA}]$) is plotted on the right axis, showing a ratio of $\text{HONO}:\text{NO}_2 < 1$, which

743 suggests OH as a secondary product.

744

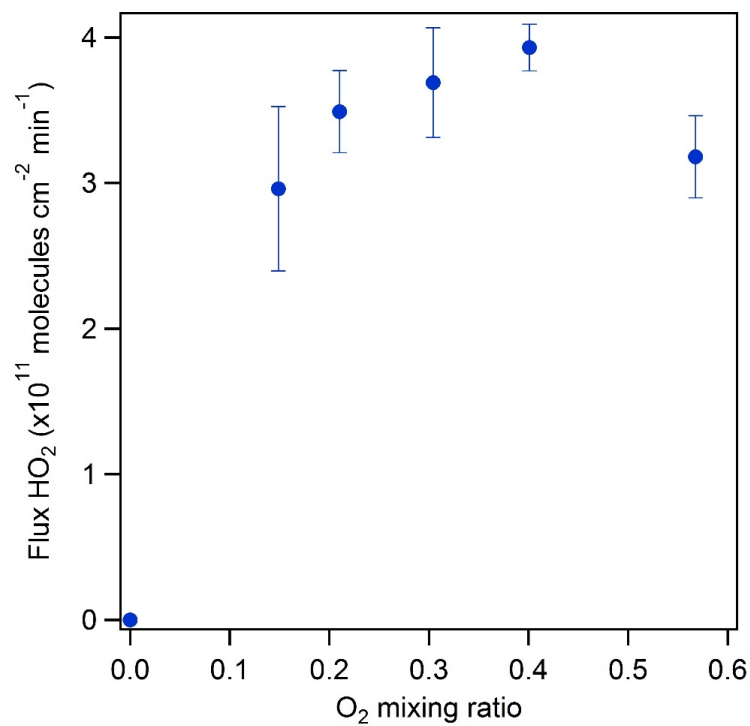


745

746

747 Figure 5. The NO loss normalized to the film surface area as a function of relative humidity.

748



749

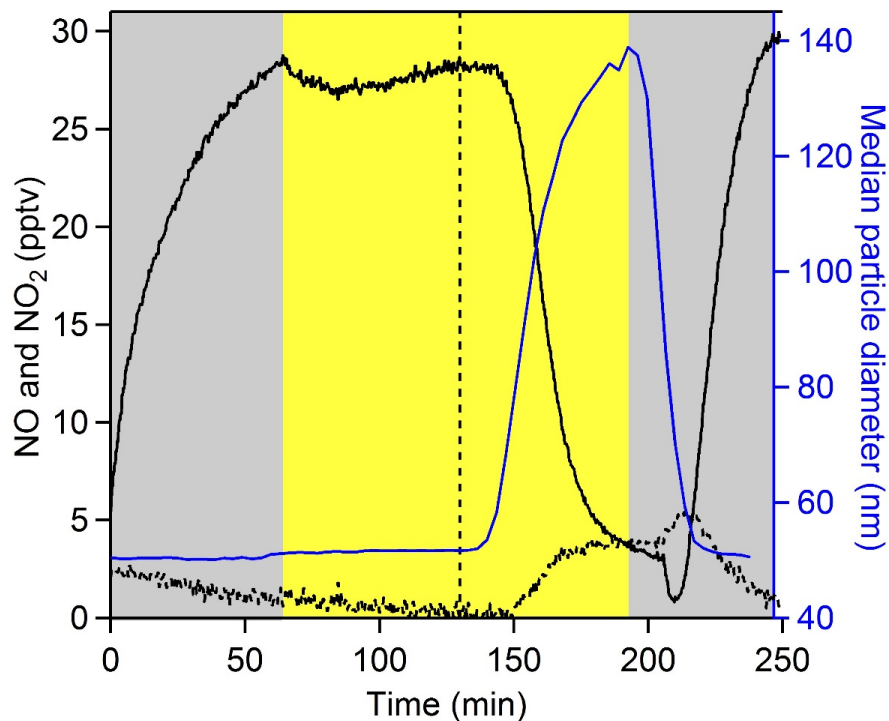
750

751 Figure 6. Measured loss of NO above a film composed of IC and CA normalized of the film
752 surface area as a function of the O₂ mixing ratio.

753



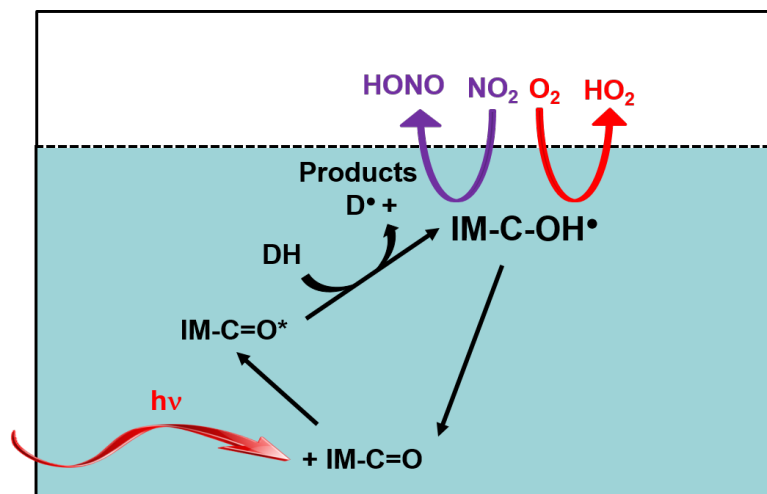
754



755

756 Figure 7. Aerosol flow tube experiments show rapid conversion of NO (solid black line) into
757 NO₂ (dashed black line) only after the time when limonene (gaseous H-donor) is added into the
758 flowtube (vertical dashed line). The gray shaded areas represent experiment in the dark, and the
759 yellow shaded area represents the experiment under light exposure. The blue line represents the
760 growth of aerosols, right axis.

761



762

763

764 Figure 8. Proposed mechanism, modified and expanded to photosensitization of IC based on
765 Canonica et al. (1995), George et al. (2005) and Aregahegn et al. (2013). The reaction in the
766 white square represents the gas-phase, and the blue square represents the aqueous phase. DH is
767 an H-donor (e.g. CA, another IC, H₂O+CA matrix to be determined from flash photolysis).

768